Real-time control of laser materials processing using deep learning

James A. Grant-Jacob,[1,*] Ben Mills,[1] and Michalis N. Zervas[1]
[1]Optoelectronics Research Centre, University of Southampton, SO17 1BJ, UK
[*]J.A.Grant-Jacob@soton.ac.uk

ABSTRACT

The plasma that is generated during laser materials processing can prevent the direct observation of the target. However, the appearance of the generated plasma is correlated with the properties of the material being ablated. Here, we show that deep learning can enable the identification of the material in real-time directly from processing camera images of the plasma, and hence can be used to automatically prevent machining beyond material boundaries. This work could have applications across laser materials processing in cases where the laser induced plasma restricts direct observation of the sample.

1. Introduction

Lasers are widely used across manufacturing and can create features at speeds that are difficult or impossible to make using mechanical processes. Lasers are used for a huge number of applications including cutting [1–3], modifying surfaces [4–6], cleaning [7,8], patterning [9,10], material removal [11,12], and depositing thin films [13–15]. Whilst laser materials processing can enable high precision manufacturing (particularly in the case for femtosecond lasers, which can result in significantly reduced heat effects), high power lasers can lead to the formation of plasma emitted from the material due to ionization [16,17]. As such, real-time imaging of the machined surface can be challenging [18,19]. To tackle this problem, new techniques are required for characterizing the surface of the sample, in real-time, during the laser-material interaction.

Deep learning is a type of artificial intelligence that uses neural networks for the modelling of complex systems [20]. Neural networks have been used widely, for example in speech recognition, image recognition, image generation and autonomous driving cars [21]. When applied to the field of laser machining [22], deep learning has been shown to be capable of defective laser weld identification [23], distortion prediction in laser additive manufacturing [24], monitoring of femtosecond laser ablation [25], and modelling fibre laser cutting [26]. Deep learning enables a data-driven approach, where the model is created directly from experimental data. Deep learning is therefore an ideal technique for optimizing and controlling laser materials processing, as it is a highly nonlinear and complex process.

Previous work has shown the application of laser-induced plasma for real-time composition monitoring of laser additive manufacturing [27], pulsed laser ablation of metals [28], and monitoring of laser welding [29]. Here, we use deep learning to enable real-time control of femtosecond laser materials processing via imaging the plasma emitted when single femtosecond laser pulses interact with the target material. Specifically, we show the ability for identification of the boundary between two different materials, in real-time, during femtosecond laser ablation. Whilst here we show examples for two adjacent materials (BiSe and quartz) and the edge of a material (glass and air), it is anticipated that any combinations of materials could be used if a neural network can identify the material from the produced plasma.

The approach demonstrated here could see applications in laser machining in many cases, for example where the translation stages have high levels of backlash and/or imprecise movement, where the target samples are part of a moving component (such as moving machinery or in a marine environment), where there is an unknown spatial distribution of the sample (such as rust on a metallic surface), or for materials where the ablation rate is less predictable. In addition, simply applying this approach may remove the need for pre-programming the stage coordinates, hence saving time and money during manufacturing.

2. Methods

A Light Conversion Pharos SP was used to produce 190 fs, 1 mJ pulses, with a central wavelength of 1030 nm. The laser pulses were focused onto the surface of the sample using a 20× Nikon objective, resulting in a maximum laser fluence of ~ 98 $mJcm^{-2}$. As shown in the schematic in Fig. 1, two cameras and two microscope objectives were used in the experiment. Camera 1 (Basler acA4112-20uc, 1914 × 1200, RGB) imaged the surface of the sample, and camera 2 (Basler daA1920-160uc, 4096 × 3000, RGB) imaged the generated plasma perpendicular to the surface of the sample. The plasma was generated along the laser axis in the opposite direction to the propagation of the laser pulses. The plasma was imaged using a 50× Olympus long working distance objective. The sample was placed on a motorized XYZ translation stage (Thorlabs) that enabled automated movement of the sample. The translation stages, shutter-controlled white light source, the cameras, and the laser were all controlled using Python, to enable automated data collection.

A stage velocity of 0.1 mms^{-1} was used to move the sample (move X, then move Y), with 10 μm of X and Y backlash corrections applied at each position, followed by a period of no movement to allow for image capture of the sample for validation. The camera recording the plasma images had an integration time of 300 ms to ensure the plume was recorded correctly even in the case of random latency in the generation of pulses from the laser (where the average time for between the computer requesting a single pulse and

laser machining was ~ 600 ms). To validate the results in this study, camera images of the sample were recorded before, during and after each incident laser pulse, resulting in a total of ~8 seconds between laser pulses. However, in a practical implementation, this validation step would not be needed, and the camera imaging the plasma could be replaced by a low-latency high-speed camera triggered directly by the laser cavity.

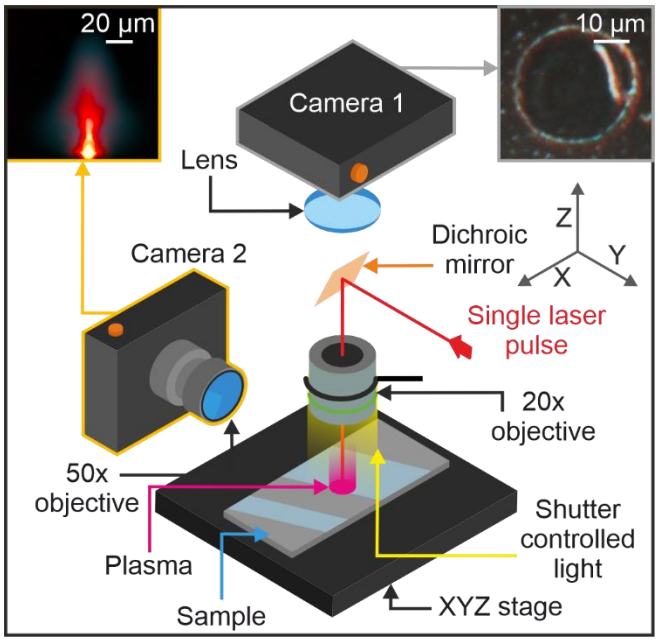

Fig. 1. (a) Schematic of the experimental setup in which laser pulses were directed onto a dichroic mirror and onto the sample, causing plasma to be emitted from the surface. Camera 1 recorded the surface before and after ablation whilst camera 2 recorded images of the plasma.

The objective of this experiment was to demonstrate that a neural network could be used, in real-time, to ensure that a scanning laser beam could be prevented from moving beyond the boundary of two adjacent materials, directly from observation of the generated plasma. This is demonstrated through two experiments. Firstly, laser pulses were scanned over the surface of a silica slide, whilst the laser was prevented from scanning beyond the edge of the silica slide. Secondly, laser pulses were scanned over the surface of a quartz substrate with regions where the quartz was coated with a 1-micron thick layer of BiSe, and the laser focus was prevented from scanning beyond the boundary of BiSe-coated-quartz and uncoated-quartz.

Surface images of the sample (camera 1) were combined with images of the plasma (camera 2) to allow the manual identification of the most appropriate label for each recorded plasma image. The labels used for the first experiment were 0 (air), 1 (boundary), and 2 (silica), and the labels for the second experiment were 0 (uncoated-quartz), 1 (boundary), 2 (BiSe-coated-quartz). This data was used to train the two convolutional neural networks (CNNs) used for this work, each of which received a plasma image and outputted a single number (i.e. the label value).

The plasma images were cropped and resized to 256 × 256 pixels, before being used as inputs. Both CNNs had 3 convolutional layers, each consisting of ReLU and max pooling sublayers, and the final layer was a regression output. The loss function was MSE, and the optimizer was ADAM [30]. No data augmentation was applied. The neural networks were trained in Python on the Microsoft Windows 10 computer (Titan Xp 12 GB, Intel i7-7700 CPU @ 3.60GHz, 64 GB RAM) used to automate the experiment. For experiment 1, the training data for initial work had labels of 0 (35 items), 1 (9 items) and 2 (26 items), whilst the further collection of data allowed for training data with labels of 0 (68 items), 1 (17 items) and 2 (53 items). For experiment 2, the training data had labels of 0 (50 items), 1 (4 items) and 2 (34 items). Training took ~ 2 minutes. Once trained, each CNN was then applied to new areas of the samples, in real-time, to prevent the laser scanning beyond the material boundaries. Due to the small size of the CNNs, the time from camera data capture to category prediction was ~ 100 ms. If the predicted value was below a threshold, then the laser was considered to have gone beyond the boundary, and the stages were automatically translated to a new line, as shown by the flow diagram in Fig. 2.

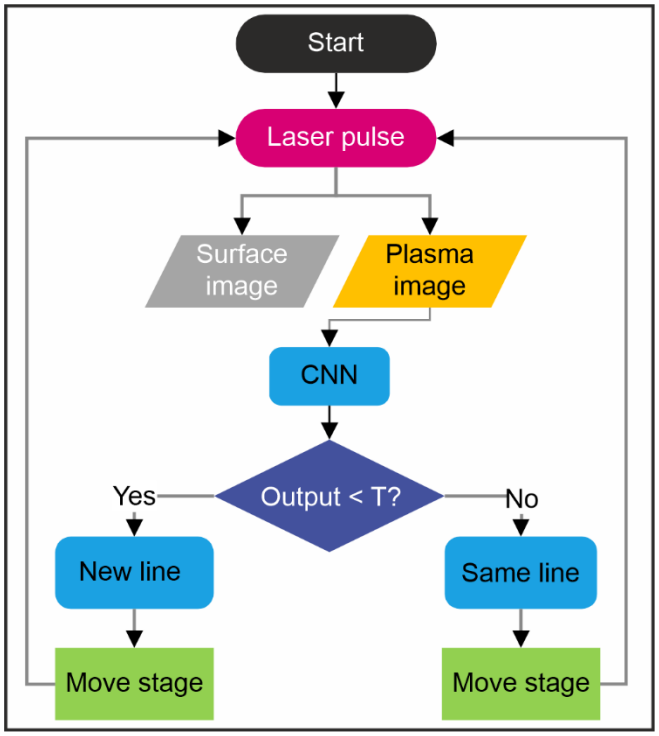

Fig. 2. Flow diagram showing the sequence of firing a laser pulse, capturing surface and plasma images, then inputting the plasma image into a CNN, which then processed the image to give an output value. If the output value was less than the threshold value (T), the stage translated to a new line. Otherwise, the stage moved to the next scan position in the current line.

3. Results and Discussion

Figure 3(a) shows the results of laser ablation of a snaking pattern beyond the edge of the silica sample, when the laser focus was not prevented from scanning beyond the edge of the sample. At the center of the laser focus for each position,

the output value of the CNN is shown as a colored circle. The dashed lines (and arrows) indicate the path and direction of the laser focus over the sample. As shown in the figure, the plasma from silica is associated with a higher predicted value than plasma generated from air. Due to the high intensity of the femtosecond laser pulse (98 $mJcm^{-2}$), ionisation of air can occur at the laser focus, hence allowing the identification of positions beyond the edge of the glass slide.

The result of laser ablation where the laser is prevented from scanning beyond the edge of the silica sample is shown in Fig. 3(b). The figure shows the laser ablation ceased once the edge of the silica had been reached (using a threshold value of 2) and the stages were automatically translated to a new line. The figure also shows example plasma images and their associated predicted values calculated in real-time, for ionizing (c) air, (d) the air/silica boundary, and (e) silica.

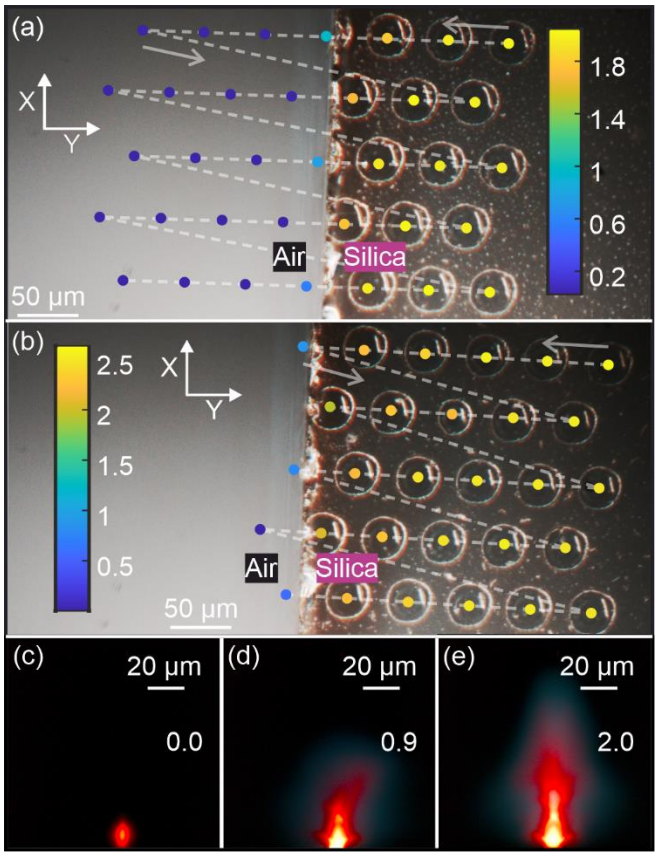

Fig. 3. Experimentally collected microscope images of laser ablation of silica and air, with the corresponding regression output values for the plasma images taken at each position displayed as solid circles in the figure, for (a) real-time control turned off (CNN trained with initial training data), and (b) real-time control turned on (CNN trained on additional data). Also shown are example plasma images and their associated predicted values for (c) air, (d) the air/silica boundary, and (e) silica.

Figure 4(a) and (b) show the result of real-time control of laser ablation around the boundary of uncoated-quartz and BiSe-coated-quartz. Example plasma images and associated predicted values as shown for (c) uncoated-quartz, (d) material boundary, and (e) BiSe-coated-quartz. The threshold values for Fig. 4 were (a) 1 and (b) 1.5, demonstrating patterning control.

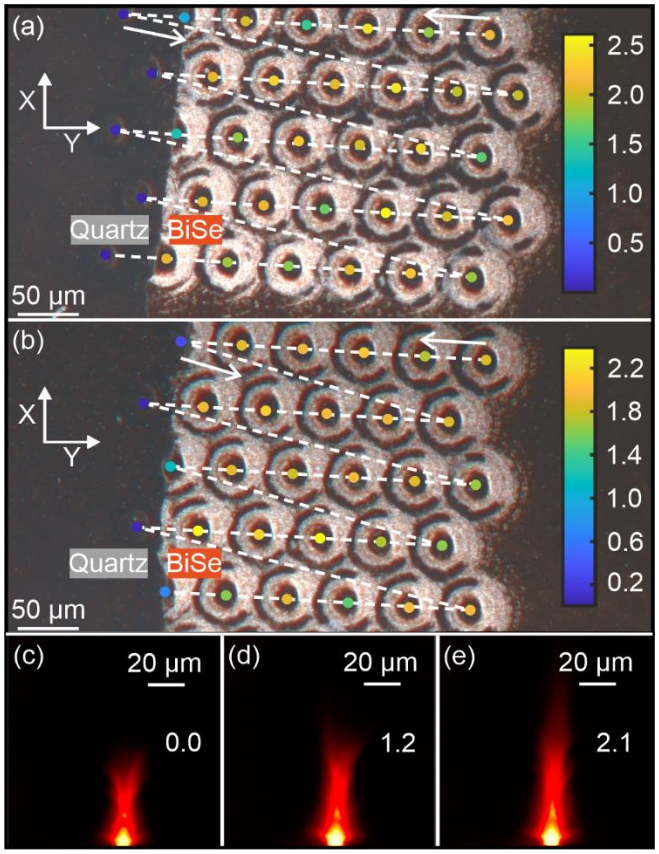

Fig. 4. Experimentally collected microscope images of laser ablation of uncoated-quartz and BiSe-coated-quartz, with the corresponding regression output values for the plasma images taken at each position displayed as solid circles in the figure, for threshold values of (a) 1 and (b) 1.5. Also shown are example plasma images and their associated predicted values for (c) uncoated-quartz, (d) the material boundary, and (e) BiSe-coated-quartz.

4. Conclusion

In conclusion, we have demonstrated the real-time control of laser materials processing of silica and BiSe-coated quartz, through processing of images of plasma generated during femtosecond ablation. The results show the application of convolutional neural networks for preventing a scanning laser focus from moving beyond material boundaries. This work could have applications across laser materials processing where direct observation of the target sample is restricted.

Declaration of Competing Interest

The authors declare no conflicts of interest.

Acknowledgements

Funding. Engineering & Physical Sciences Research Council (EP/W028786/1, EP/T026197/1, EP/P027644/1).

Data availability

Data underlying the results presented in this paper are available at https://doi.org/10.5258/SOTON/D2705.

References

[1] Wetzig A, Herwig P, Hauptmann J, Baumann R, Rauscher P, Schlosser M, et al. Fast laser cutting of thin metal. Procedia Manuf 2019;29:369–74.

[2] Fuchs AN, Schoeberl M, Tremmer J, Zaeh MF. Laser cutting of carbon fiber fabrics. Phys Procedia 2013;41:372–80.

[3] Shin JS, Oh SY, Park H, Chung CM, Seon S, Kim TS, et al. High-speed fiber laser cutting of thick stainless steel for dismantling tasks. Opt Laser Technol 2017;94:244–7. https://doi.org/10.1016/j.optlastec.2017.03.040.

[4] Tian YS, Chen CZ, Li ST, Huo QH. Research progress on laser surface modification of titanium alloys. Appl Surf Sci 2005;242:177–84.

[5] Jeyaprakash N, Yang C-H, Kumar DR. Laser Surface Modification of Materials. Practical Applications of Laser Ablation, IntechOpen London, UK; 2020.

[6] Grant-Jacob JA, Mills B, Eason RW. Parametric study of the rapid fabrication of glass nanofoam via femtosecond laser irradiation. J Phys D Appl Phys 2014;47. https://doi.org/10.1088/0022-3727/47/5/055105.

[7] Tam AC, Leung WP, Zapka W, Ziemlich W. Laser-cleaning techniques for removal of surface particulates. J Appl Phys 1992;71:3515–23. https://doi.org/10.1063/1.350906.

[8] Zapka W, Tam AC, Ziemlich W. Laser cleaning of wafer surfaces and lithography masks. Microelectron Eng 1991;13:547–50.

[9] Heath DJ, Grant-Jacob JA, Feinaeugle M, Mills B, Eason RW. Sub-diffraction limit laser ablation via multiple exposures using a digital micromirror device. Appl Opt 2017;56:6398–404. https://doi.org/10.1364/AO.56.006398.

[10] Solomon JM, Ahmad SI, Dave A, Lu L-S, HadavandMirzaee F, Lin S-C, et al. Ultrafast laser ablation, intrinsic threshold, and nanopatterning of monolayer molybdenum disulfide. Sci Rep 2022;12:6910. https://doi.org/10.1038/s41598-022-10820-w.

[11] Seo C, Ahn D, Kim D. Removal of oxides from copper surface using femtosecond and nanosecond pulsed lasers. Appl Surf Sci 2015;349:361–7.

[12] Daurelio G, Chita G, Cinquepalmi M. Laser surface cleaning, de-rusting, de-painting and de-oxidizing. Applied Physics A 1999;69:S543–6.

[13] Ashfold MNR, Claeyssens F, Fuge GM, Henley SJ. Pulsed laser ablation and deposition of thin films. Chem Soc Rev 2004;33:23–31.

[14] Prentice JJ, Grant-Jacob JA, Kurilchik SV, Mackenzie JI, Eason RW. Particulate reduction in PLD-grown crystalline films via bi-directional target irradiation. Appl Phys A Mater Sci Process 2019;125. https://doi.org/10.1007/s00339-019-2456-5.

[15] Grant-Jacob JA, Beecher SJ, Riris H, Anthony WY, Shepherd DP, Eason RW, et al. Dynamic control of refractive index during pulsed-laser-deposited waveguide growth. Opt Mater Express 2017;7:4073–81.

[16] Amoruso S, Bruzzese R, Pagano C, Wang X. Features of plasma plume evolution and material removal efficiency during femtosecond laser ablation of nickel in high vacuum. Applied Physics A 2007;89:1017–24.

[17] Bogaerts A, Chen Z. Effect of laser parameters on laser ablation and laser-induced plasma formation: A numerical modeling investigation. Spectrochim Acta Part B At Spectrosc 2005;60:1280–307.

[18] Kawahito Y, Matsumoto N, Mizutani M, Katayama S. Characterisation of plasma induced during high power fibre laser welding of stainless steel. Science and Technology of Welding and Joining 2008;13:744–8.

[19] Lewis GK, Dixon RD. Plasma monitoring of laser beam welds. Laser 1984;13:2.

[20] LeCun Y, Bengio Y, Hinton G. Deep learning. Nature 2015;521:436.

[21] Talpes E, Sarma DD, Venkataramanan G, Bannon P, McGee B, Floering B, et al. Compute Solution for Tesla's Full Self-Driving Computer. IEEE Micro 2020;40:25–35. https://doi.org/10.1109/MM.2020.2975764.

[22] Mills B, Grant-Jacob J. Lasers that learn: the interface of laser machining and machine learning. IET Optoelectronics 2021.

[23] Buongiorno D, Prunella M, Grossi S, Hussain SM, Rennola A, Longo N, et al. Inline defective laser weld identification by processing thermal image sequences with machine and deep learning techniques. Applied Sciences 2022;12:6455.

[24] Francis J, Bian L. Deep learning for distortion prediction in laser-based additive manufacturing using big data. Manuf Lett 2019;20:10–4.

[25] Mills B, Heath DJ, Grant-Jacob JA, Xie Y, Eason RW. Image-based monitoring of femtosecond laser machining via a neural network. Journal of Physics: Photonics 2018;1:015008.

[26] Courtier AF, McDonnell M, Praeger M, Grant-Jacob JA, Codemard C, Harrison P, et al. Modelling of fibre laser cutting via deep learning. Opt Express 2021;29:36487–502. https://doi.org/10.1364/OE.432741.

[27] Song L, Huang W, Han X, Mazumder J. Real-time composition monitoring using support vector regression of laser-induced plasma for laser additive manufacturing. IEEE Transactions on Industrial Electronics 2016;64:633–42.

[28] Stafe M, Negutu C. Real-time monitoring of the pulsed laser ablation of metals using ablation plasma spectroscopy. Plasma Chemistry and Plasma Processing 2012;32:643–53.

[29] Li L, Brookfield DJ, Steen WM. Plasma charge sensor for in-process, non-contact monitoring of the laser welding process. Meas Sci Technol 1996;7:615.

[30] Kingma DP, Ba J. Adam: A method for stochastic optimization. ArXiv Preprint ArXiv:14126980 2014.